Microbial community production, respiration, and structure of the microbial food web of an ecosystem in the northeastern Atlantic Ocean

Anne Maixandeau,[1] Dominique Lefèvre,[1] Hera Karayanni,[1,2] Urania Christaki,[3,4] France Van Wambeke,[1] Melilotus Thyssen,[1] Michel Denis,[1] Camila I. Fernández,[5] Julia Uitz,[6] Karine Leblanc,[5] and Bernard Quéguiner[5]

[1] Gross community production (GCP), dark community respiration (DCR), and the biomass of the different size classes of organisms in the microbial community were measured in the northeastern Atlantic basin as part of the Programme Océan Multidisciplinaire Méso Echelle (POMME) project. The field experiment was conducted during three seasons (winter, spring, and late summer–fall) in 2001. Samples were collected from four different mesoscale structures within the upper 100 m. GCP rates increased from winter (101 ± 24 mmol O_2 m^{-2} d^{-1}) to spring (153 ± 27 mmol O_2 m^{-2} d^{-1}) and then decreased from spring to late summer (44 ± 18 mmol O_2 m^{-2} d^{-1}). DCR rates increased from winter (-47 ± 18 mmol O_2 m^{-2} d^{-1}) to spring (-97 ± 7 mmol O_2 m^{-2} d^{-1}) and then decreased from spring to late summer (50 ± 7 mmol O_2 m^{-2} d^{-1}). The onset of stratification depended on latitude as well as on the presence of mesoscale structures (eddies), and this largely contributed to the variability of GCP. The trophic status of the POMME area was defined as net autotrophic, with a mean annual net community production rate of $+38 \pm 18$ mmol O_2 m^{-2} d^{-1}, exhibiting a seasonal variation from $+2 \pm 20$ mmol O_2 m^{-2} d^{-1} to $+57 \pm 20$ mmol O_2 m^{-2} d^{-1}. This study highlights that small organisms (picoautotrophs, nanoautotrophs, and bacteria) are the main organisms contributing to biological fluxes throughout the year and that episodic blooms of microphytoplankton are related to mesoscale structures.

Citation: Maixandeau, A., et al. (2005), Microbial community production, respiration, and structure of the microbial food web of an ecosystem in the northeastern Atlantic Ocean, *J. Geophys. Res.*, *110*, C07S17, doi:10.1029/2004JC002694.

1. Introduction

[2] The oceanic ecosystem contributes to approximately half of the primary production of the biosphere [*Field et al.*, 1998]. The balance between gross primary production and community respiration in oceanic systems determines whether the biological pump acts as a net source or sink of carbon [*Williams*, 1993]. However, this balance is variable with geographical, temporal and seasonal scales [*Geider*, 1997; *del Giorgio et al.*, 1997; *Williams*, 1998; *Duarte and Agusti*, 1998; *del Giorgio and Duarte*, 2002], highlighting the need to study ecosystem functioning over smaller scales in order to determine the trophic status on a global scale [*Serret et al.*, 1999; *González et al.*, 2001, 2002].

[3] Microbial community production and respiration depend on the trophic structure and its effect on ecosystem functioning [*Azam et al.*, 1983; *Cotner and Biddanda*, 2002]. More recently, comparative analyses in aquatic microbial ecology have focused on community functioning in relation to the structure and dynamics of the food web. This is dependent on temperature, nutrient availability and the abundance and productivity of primary producers [*Gasol and Duarte*, 2000].

[4] The controlling variables are affected by the surrounding hydrodynamics. For example, physical processes control the injection of nutrients into the productive layer [*Falkowski et al.*, 1991; *Oschlies and Garçon*, 1998]. Turbulence controls the microbial community structure [*Margalef*, 1978], food web interactions [*Cullen et al.*, 2002], and light availability [*Rodríguez et al.*, 2001].

[5] This study focuses on an ecosystem located in the north east Atlantic Ocean, between the Azores and Portugal. The area is characterized by the formation of northeast

---

[1]Laboratoire de Microbiologie, Géochimie et Ecologie Marines, Centre National de la Recherche Scientifique/Institut National des Sciences de l'Univers, UMR 6117, Centre d'Océanologie de Marseille, Université de la Méditerranée, Marseille, France.

[2]Also at Hellenic Centre for Marine Research, Anavissos, Greece.

[3]Hellenic Centre for Marine Research, Anavissos, Greece.

[4]Now at Université du Littoral Côte d'Opale/Maison de la Recherche en Environnement Naturel, CNRS/INSU, UMR 8013 "Ecosystèmes Littoraux et Côtiers," Wimereux, France.

[5]Laboratoire d'Océanographie et de Biogéochimie, Centre National de la Recherche Scientifique/Institut National des Sciences de l'Univers, UMR 6535, Centre d'Océanologie de Marseille, Université de la Méditerranée, Marseille, France.

[6]Laboratoire d'Océanographie de Villefranche, Observatoire Océanologique, Villefranche-sur-mer, France.
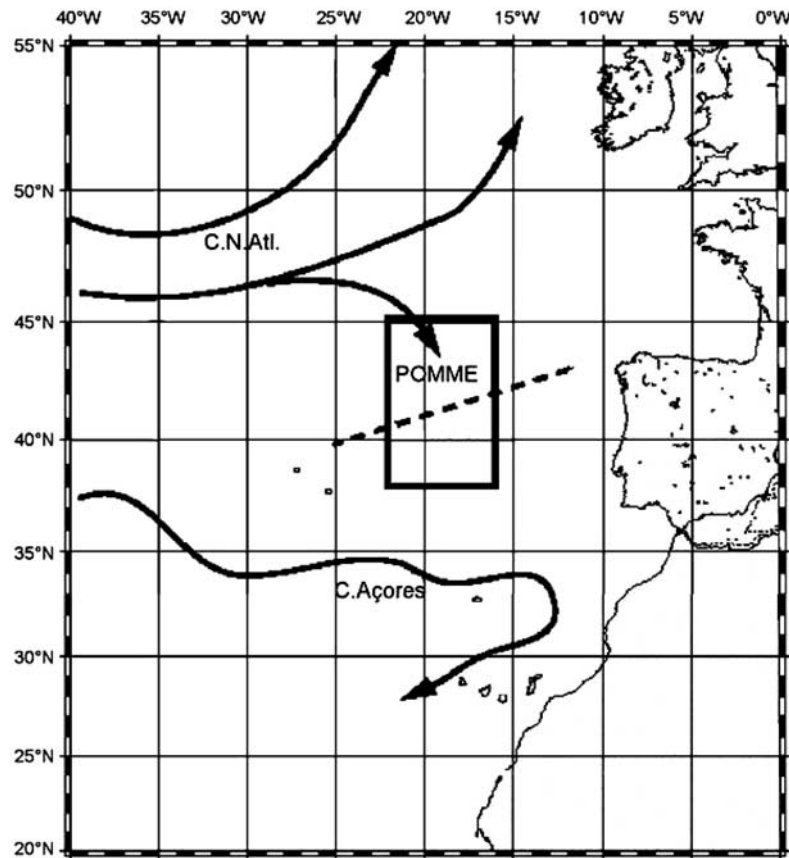
Figure 1. Study area for Programme Océan Multidisciplinaire Méso Echelle (POMME) 2000–2001 in the North Atlantic Ocean. The rectangle represents the study area, and the dotted line indicates the approximate zone of discontinuity in the winter mixed layer depth. Oceanographic cruises are as follows: POMME 1 (leg 2, 27 February–20 March 2001), POMME 2 (leg 2, 16 April–7 May 2001), and POMME 3 (leg 2, 17 September–10 October 2001).

Atlantic modal waters in winter and their subsequent subduction in spring [*Paillet and Arhan*, 1996], and presents a number of cyclonic and anticyclonic eddies [*Arhan et al.*, 1994]. An abundant supply of nutrients stimulates the ecosystem productivity, making this area one of the most biologically productive regions [*Falkowski et al.*, 1991; *McGillicuddy et al.*, 1998; *Oschlies and Garçon*, 1998].

[6] Biological fluxes were studied during the Programme Océan Multidisciplinaire Méso Echelle (POMME) project. Microbial community production and respiration in this area have previously been studied using data of production and respiration from surface water (5 m [*Maixandeau et al.*, 2005]). This previous study has highlighted the seasonal cycle and mesoscale variability of the microbial community production and respiration in relation with the hydrological context and the time lag between the two processes [*Maixandeau et al.*, 2005].

[7] In this study, several parameters were analyzed simultaneously to provide an overview of the microbial ecosystem functioning: (1) vertical fluxes of gross community production (GCP) and dark community respiration (DCR) rates and (2) microbial community composition, based on estimates of autotrophic and heterotrophic bio-

masses of the main components of the microbial food web (for heterotrophs: bacteria, flagellates and ciliates, and for autotrophs: picophytoplancton, nanophytoplancton, dinoflagellates, coccolithophores, diatoms and silicoflagellates). These parameters were measured in winter, spring and late summer within selected hydrodynamical structures. We attempt to explain the spatial variability of biological processes with respect to particular hydrodynamical features and to the structure of the microbial community at the different seasons and finally we determine the trophic status of the area.

2. Materials and Methods

2.1. Study Area

[8] This study was carried out during the POMME project in the region between the Azores and Portugal (Figure 1). The study area covers the North Atlantic Drift Province (NADR) and the transition zone from the NADR to the warmer and more saline waters of the eastern part of the North Atlantic Subtropical Gyre Province (NAST (E)) [*Longhurst et al.*, 1995]. This area is characterized by the formation of mesoscale eddies and by the subduction of modal waters during the thermocline installation. The

Table 1. Schedule, Position of Sites, and Hydrological Context[a]

	Winter	Spring	Late Summer
Site 1	18.7°W−40.1°N	19.8°W−39.8°N	19.1°W−40.1°N
HS	anticyclonic eddy (A2)	anticyclonic eddy (A2)	anticyclonic eddy (A3-1)
$Z_m - Z_e$	26 ± 13 (4)−57 ± 3 (4)	21 ± 6 (3)−45 ± 2 (3)	34 ± 3 (3)−86 ± 7 (3)
DIN	3.0 ± 0.1	0.8 ± 0.2	0.04 ± 0.01
$Z\Delta NO_3 - \Delta NO_3$	90−0.1	90−9.2	70−3.6
Site 2	18.6°W−41.1°N	19.7°W−41.9°N	19.8°W−42.2°N
HS	frontal zone (FZ)	cyclonic eddy (C4)	in the vicinity of C4
$Z_m - Z_e$	71 ± 20 (3)−54 ± 1 (3)	33 ± 3 (3)−44 ± 4 (3)	39 ± 5 (3)−93 ± 2 (3)
DIN	4.2 ± 0.1	2.2 ± 0.6	0.01 ± 0.0
$Z\Delta NO_3 - \Delta NO_3$	105−1.1	32−3.3	70−4.0
Site 3	19.2°W−41.8°N	17.7°W−42.1°N	22°W−41.5°N
HS	cyclonic eddy (C4)	no activity (saddle point (SP))	cyclonic eddy (C4)
MLD − ELD	48 ± 16 (3)−51 ± 2 (3)	31 ± 16 (3)−49 ± 1 (3)	37 ± 7 (3)−90 ± 4 (3)
DIN	4.9 ± 0.2	2.4 ± 0.2	0.14 ± 0.0
$Z\Delta NO_3 - \Delta NO_3$	125−1.4	80−3.4	65−6.8
Site 4	17.4°W−43.3°N	18.8°W−43.3°N	18°W−42.4°N
HS	anticyclonic eddy (A1)	anticyclonic eddy (A1)	in the vicinity of C3-1
MLD − ELD	98 ± 7 (3)−44 ± 1 (3)	61 ± 5 (3)−48 ± 2 (3)	39 ± 5 (3)−88 ± 2 (3)
DIN	5. 0 ± 0.2	3.2 ± 1.6	0.03 ± 0.04
$Z\Delta NO_3 - \Delta NO_3$	80−0.5	65−4.0	65−6.7

[a]The position of each site was defined during the cruise with the model of hydrodynamical circulation Système Océanique de Prévision en Atlantique Nord-Est (SOPRANE). Abbreviations are as follows: HS, hydrodynamical structure; Z_m, mixed layer depth (m ± sd, n); Z_e, euphotic layer depth (m ± sd; n); DIN, average concentration in the mixed layer (μmol dm^{-3}); $Z\Delta NO_3$, depth of the nitracline (m); ΔNO_3, gradient of the nitracline (μmol dm^{-3}).

POMME project consisted of three oceanographic cruises in winter (P1), spring (P2) and late summer−fall (P3) 2001 [*Mémery et al.*, 2005]. Each cruise consisted of two legs. During the first leg of each cruise, Eulerian sampling was carried out over 20 days for 79, 81 and 83 stations during P1, P2 and P3. *Maixandeau et al.* [2005] reviews the surface layer data from legs 1 whereas this study focuses on data collected during legs 2 (Table 1). During the second leg of each cruise, a Lagrangian sampling strategy was carried out; 8 depths were sampled in the upper 100 m in four different hydrodynamical structures. The different mesoscale structures were identified as well as their weekly displacement throughout the POMME survey resulting in a nomenclature of mesoscale structures [*Mémery et al.*, 2005]. The hydrodynamical structures were followed by the deployment of a drifting sediment trap for 48 h at each site [*Mémery et al.*, 2005] (Figure 2). Site positions were defined using the Système Océanique de Prévision en Atlantique Nord-Est (SOPRANE) circulation model which was updated with conductivity-temperature-depth (CTD) data from leg 1 and by using an acoustic Doppler current profiler (ADCP) transect carried out simultaneously in the area during the second leg. The hydrological context for each site is summarized in Table 1. This study focuses on two anticyclonic eddies (A1 and A2) and one cyclonic eddy (C4) that were visible during more than one cruise (A1, 10 months; A2 and C4, 6 months).

[9] Sampling was carried out using a Seabird® SBE 9 CTD rosette sampler equipped with 21 12 dm^3 Niskin bottles. Prior to the first sampling, the Niskin bottles were cleaned with 0.2% HCl and rinsed with distilled water. Rubber O-rings were replaced with Viton® and the original rubber tubes replaced with silicon to minimize contamination by organic materials.

2.2. Biological Fluxes

[10] Rates of gross community production (GCP), dark community respiration (DCR) and net community production (NCP) were estimated from changes in the dissolved oxygen concentration over 24 hour incubations which were carried out on an in situ rig. During legs 2, rates were measured at up to eight depths (5, 20, 30, 40, 50, 60, 80 and 100 m), to cover the euphotic zone. Three sets of four replicates were collected into 125 cm^3 borosilicate glass bottles. A first set of samples was fixed immediately (using Winkler reagents) to measure the oxygen concentration at time 0; the second set was packed in an opaque dark material to ensure a total obscurity; no modification was made to the last set. The samples from the last two sets were placed on an in situ rig, to the depth at which they were sampled, and incubated for 24 hours, from 0600 LT to 0600 LT the following day, prior to being fixed. Dissolved oxygen concentration was measured using an automated high-precision Winkler titration system linked to a photometric end point detector [*Williams and Jenkinson*, 1982]. NCP was calculated as the difference in the dissolved oxygen concentration between "light" incubated samples and "time 0" samples. DCR was calculated as the difference between "dark" incubated samples and "time 0" samples. DCR rates are expressed as a negative O_2 flux. GCP is the difference between NCP and DCR [*Gaarder and Gran*, 1927]. Results presented in this study are integrated data over the upper 80 or 100 m, depending on the last sampled depth. Standard errors on the rates are calculated from the standard deviation of quadruple samples sets. The mean standard error obtained was ±0.3 mmol O_2 m^{-3} d^{-1}.

2.3. Biogeochemical Context

[11] Samples for nutrient analysis (NO_3^-, NO_2^-, NH_4^+, PO_4^-) were collected into 20 cm^3 polyethylene bottles that had been prerinsed with 10% hydrochloric acid. Samples were analyzed immediately after sampling using a Technicon Auto Analyser following the protocol of *Armstrong et al.* [1967] and *Tréguer and LeCorre* [1975]. We refer to the total dissolved inorganic nitrogen (DIN) as the sum of (NO_3^-, NO_2^-, NH_4^+). The depth of the euphotic layer (Z_e) was calculated from the concentration of total chlorophyll *a* (T*chla*) profiles using the model developed by *Morel and*
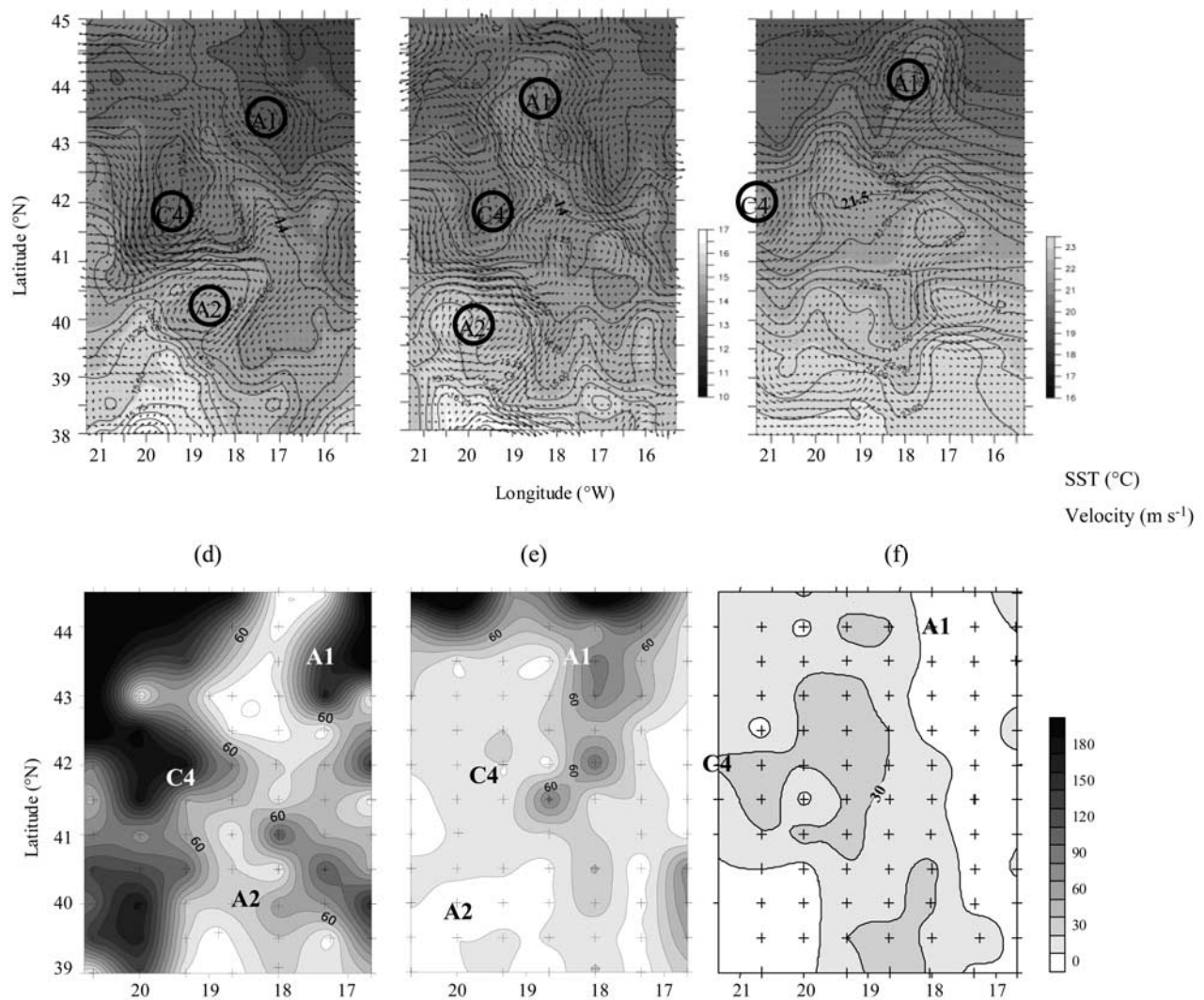
Figure 2. Contour plot of sea surface temperature at 5 m and the geostrophic current velocity at 50 m, represented by black arrows (reference: 1 m s^{-1}) for (a) winter, (b) spring, and (c) late summer. Spatial distribution of the mixed layer depth (MLD) (in meters) for (d) winter, (e) spring, and (f) late summer. MLD is defined by an excess density >0.002 kg m^{-3} m^{-1}. A1 and A2 indicate the location of anticyclonic eddies, and C4 indicates the location of a cyclonic eddy.

Maritorena [2001] where the *T*chl*a* content in the water column was calculated by integrating *T*chl*a* with depth. Z_e was finally determined through an iterative process described by *Morel and Berthon* [1989]. The depth of the mixed layer, Z_m, was estimated from excess density profiles derived from CTD casts (average value of four to five profiles per site). It corresponds to the depth were the density is greater than the surface one by more than 0.02 kg m^{-3}. Values were estimated from the average of the vertical profiles carried out at each site and where Z_e was determined.

2.4. Flow Cytometry Analyses

[12] Collected seawater samples were preserved in paraformaldehyde (2% final concentration), frozen and stored in liquid nitrogen until analysis in the laboratory. The abundance of *Prochlorococcus*, *Synechococcus*, pico- and nanophytoplankton and high and low nucleic acid bacteria (HNA and LNA, respectively) were determined using flow cytometry (Cytoron Absolute, Diagnostic System) as described by *Grégori* [2001] and *Dubreuil* [2003].

2.5. Microphytoplankton Abundance

[13] Samples were collected in 125 cm^3 inactinic bottles and fixed with Lugol for diatom enumeration and with formol for flagellate and coccolithophore counts [*Throndsen*, 1978]. Identification and enumeration of the main phytoplankton groups (diatoms, coccolithophores, silicoflagellates, dinoflagellates) were conducted in a sedimentation chamber (50 cm^3) at 100×, 200× and 400× magnifications using an inverted microscope (Nikon, TE 300 according to *Utermöhl* [1931]).

2.6. Ciliate and Heterotrophic Nanoflagellate Counts

[14] For ciliate enumeration, 250 cm^3 samples were obtained from eight depths in the surface layer (0–100 m).

After gentle mixing, the samples were fixed with borax-buffered formaldehyde 2% (final concentration) and stored in the dark at 4°C until analysis in the laboratory. Subsamples of 100 cm^3 were concentrated by sedimentation. Cells were counted using epifluorescence microscopy on an Olympus IX–70 inverted microscope at 400×. Correction factors were applied in order to compensate for cell losses due to fixation [Karayanni, 2004]. To enumerate heterotrophic nanoflagellates (HNAN) 20–30 cm^3 samples were fixed with 1% (final concentration) ice-cold glutaraldehyde. Samples were filtered onto 0.6 μm polycarbonate filters, stained with DAPI and stored at −20°C until counting. HNAN were enumerated using an Olympus PROVIS epifluorescence microscope at 1000×. This group of organisms (heterotrophic nanoflagellates and ciliates) is referred as "micrograzers."

2.7. Biomass Estimations

[15] The abundance of *Synechococcus* and *Prochlorococcus* was converted into carbon biomass using the estimations of 250 fg C $cell^{-1}$ [Kana and Glibert, 1987] and 49 fg C $cell^{-1}$, respectively [Caillau et al., 1996]. The abundance of different microphytoplanktonic groups were converted into biomass according to Strathmann [1967]. Average coccolithophores biovolumes were 523 $μm^3$, during P1, P2 and P3. Average biovolumes for dinoflagellates were 7559 $μm^3$ during P1, and P3, 1840 $μm^3$ during P2 at site 2 and 3, 12432 $μm^3$ during P2 at site 1, and, 11867 $μm^3$ during P2 at site 4. Diatoms biovolumes were varying upon the cruise: 4710 $μm^3$ during P1, P2 and P3 (A2 and A3-1), 57 $μm^3$ during P3 (C4), 2384 $μm^3$ during P3 (vicinity of C4). Silicoflagellates biovolumes were the same for all three cruises: 1766 $μm^3$. Biovolume conversion into carbon biomass were $\log C = 0.758(\log V) - 0.422$ for diatoms and $\log C = 0.866(\log V) - 0.460$ for other phytoplanktonic groups [Strathmann, 1967].

[16] Bacterial abundance was converted into carbon biomass using a factor of 15 fg C $cell^{-1}$ [Caron et al., 1995]. Biovolumes for all ciliate taxa, heterotrophic and autotrophic nanoflagellates were calculated using the linear measured dimensions of cells, and equations were applied depending on cell shape (sphere, prolate spheroid or cone) [Karayanni et al., 2005]. The biovolumes for picoeucaryotes were calculated assuming an average diameter of 1.8 μm. Biovolumes of heterotrophic and autotrophic nanoflagellates and autotrophic picoeucaryotes were then converted into biomass by applying a conversion factor of 220 fg C $μm^{-3}$ [Børsheim and Bratbak, 1987]. Biovolumes of ciliates were converted into biomass using a conversion factor of 190 fg C $μm^{-3}$. For autotrophic nanoflagellates (PNAN), we used cytometric counts but applied a mean biovolume cell factor per cruise obtained by measuring cells by epifluorescence microscopy. Final conversion factors were 0.67 pg C $cell^{-1}$ for picoeucaryotes; 5.67, 3.95 and 3.50 pg C $cell^{-1}$ for autotrophic nanoflagellates in winter, spring and late summer, respectively. Results presented for bacterial biomass are integrated data over the upper 80 or 100 m, the depth on the last depth sampled.

[17] The relative error associated with the estimates of autotroph and heterotroph biomasses was 15% for the HNAN and PNAN, ciliates and microphytoplankton, 5% for bacteria, *Synechococcus* and *Prochlorococcus*. This error includes only cell counts, excluding the errors associated with the biovolume determination and the biovolume-carbon conversion.

2.8. Autotrophic and Heterotrophic Indices

[18] Oxygen fluxes were converted into CO_2 fluxes using a different photosynthetic quotient (PQ) for each season (winter: 1.4; spring: 1.3; late summer: 1.1). Indeed, nitrate stocks strongly diminished over the three seasons [Fernández et al., 2005a] (Table 1), and it has been shown that PQ values were higher when the main source of inorganic nitrogen available was nitrate [Laws, 1991]. The respiratory quotient (RQ) used was 0.8 for all data, which was derived from a previous study in the eastern North Atlantic [Robinson et al., 2002]. Carbon fixation rates (GCP) were then normalized to autotrophic biomass (defined as the autotrophic index) and respiration rates (DCR) were normalized to heterotrophic biomass (defined as the heterotrophic index) and expressed in d^{-1}. The autotrophic index is representative of the specific growth rate of the whole phytoplankton community whereas the heterotrophic index is representative of a specific remineralization rate. Care should be taken in interpreting this latter index, since DCR also includes both autotrophic and heterotrophic respiration; therefore the index overestimates the specific remineralization rate. The use of these indices will help to examine if an increase of GCP (or DCR) is due to an increase of the biomass responsible of the autotrophic activity (or heterotrophic activity), or to an increase of specific growth rates (or specific remineralization rate), or both.

2.9. Statistical Analysis

[19] Each seasonal data sets (data measured at each depth and at each site, from the surface to the deepest depth sampled for rate determination, 80 or 100 m) were analyzed using a principal component analysis (PCA) [Legendre and Legendre, 1998]. Statistical analyses were made on the following variables: rates (GCP, DCR), carbon biomass of the micro-organism categories, depth, temperature and inorganic nitrogen, in order to determine the covariability between rates, organisms and the main environmental variables. The statistical analyses were made on discrete volumetric data. The PCA is based on the partial correlation between variables and synthesizes the results on two (or more) main factors, explaining a large percentage of the total variance.

3. Results

3.1. Hydrological Context

[20] The hydrological context during the legs 1 of each cruise is presented by Fernández et al. [2005a]. The circulation is further described by Assenbaum and Reverdin [2005] and Gaillard et al. [2005] and the associated thermocline water masses in Reverdin et al. [2005]. Mesoscale structures were investigated over 48 hours during legs 2 (Table 1). Only the cyclonic site (C4) was sampled during the three cruises (Table 1). The southern area (south of 41°N), was less ventilated, characterizing these southern mesoscale structures. The mixed layer depth (Z_m) during
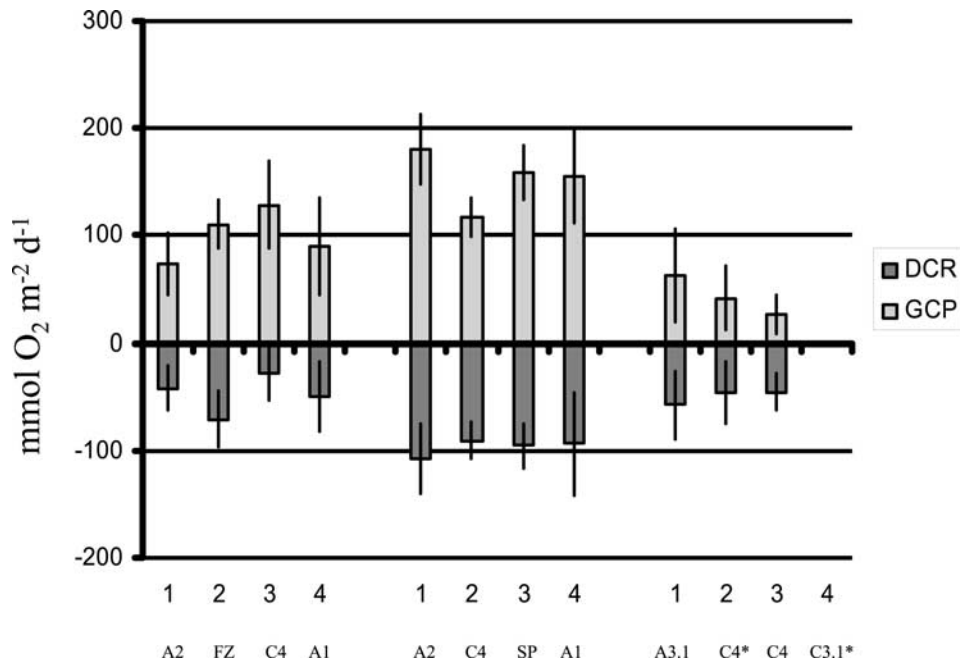
Figure 3. Integrated gross community production (GCP) and dark community respiration (DCR) (mmol O_2 m^{-2} d^{-1}) during winter, spring, and late summer. The hydrodynamical structure identification is mentioned above the site number. An asterisk indicates that measurements were made in the vicinity of the associated hydrodynamical structure.

winter was strongly variable and ranged from 26 ± 13 m (A2) to 98 ± 7 m (A1). During the spring site studies, Z_m (Table 1) ranged from 21 ± 6 m at the southern cyclonic eddy (A2) to 61 ± 5 m at the northern anticyclonic eddy (A1). This latitudinal gradient of Z_m was also found during the legs 1 [*Fernández et al.*, 2005a], as well as in modeling studies [*Paci et al.*, 2005]. Z_m was less variable in late summer and ranged from 34 ± 3 m (A3-1) to 39 ± 5 m (C3-1). The euphotic layer depth (Z_e) in winter varied with latitude and ranged from 57 ± 3 m in the south (site 1) to 44 ± 1 m in the north (site 4). Z_e did not present a similar variability between sites during the spring and late summer cruises and averaged 47 ± 5 m and 89 ± 8 m respectively (Table 1).

[21] The mean total dissolved inorganic nitrogen concentrations (DIN, i.e., sum of NO_2^-, NO_3^- and NH_4^+) presented a latitudinal gradient during the winter and spring periods (Table 1). Within Z_m, mean DIN ranged from 3.0 ± 0.1 μM (mean ± sd) to 5.0 ± 0.2 μM in winter (average concentration in the mixed layer). The nitracline depth ranged from 80 m (A1) to 125 m (C4), with a gradient less than 1.5 μM. During spring DIN ranged from 0.8 ± 0.2 μM to 3.2 ± 1.6 μM; the nitracline depth range from 32 m (C4) to 90 m (A2), and the nitracline gradient ranged from 3.3 to 9.2 μM. In late summer, the mixed layer was depleted in DIN except at C4 with DIN = 0.14 ± 0.0 μM. The nitracline depth ranged from 65 m (C4 and C3-1) to 70m (A3-1 and C4), and the nitracline gradient ranged from 3.6 to 6.8 μM (Table 1). The nitracline gradient value and the nitracline depth exhibit the potential limitation for primary production. It should be noted that during winter, the large difference is observed between Z_m and the nitracline depth, also that the nitracline gradient

values were small, whereas during spring (or late summer), due to the onset (or presence) of a thermocline, DIN values were significantly higher below Z_m than in the mixed layer (5.6 ± 1.2 μM and 4.4 ± 1.5 μM mean values for all sites, respectively).

3.2. Biological Fluxes

[22] In winter, the integrated rates of GCP and DCR (Figure 3) varied between sites. The highest GCP values were recorded in the frontal zone and in the cyclonic eddy C4 (128.7 ± 40.6 and 110.5 ± 22.0 mmol O_2 m^{-2} d^{-1}, respectively) and the lowest values were associated to anticyclonic gyres A1 and A2. DCR did not reflect this GCP variability, the lowest values being related to eddies A2 and C4. The frontal zone presented the highest values of DCR (−70.5 ± 26.2 mmol O_2 m^{-2} d^{-1}). At the cyclonic eddy (C4) the highest GCP value was associated to the lowest DCR value (−28.2 ± 25.3 mmol O_2 m^{-2} d^{-1}).

[23] Both GCP and DCR increased from winter to spring, but at the four sites investigated during P2, values were almost constant: the mean GCP and DCR values were 152.8 ± 26.6 mmol O_2 m^{-2} d^{-1} and −96.7 ± 7.4 mmol O_2 m^{-2} d^{-1}, respectively. No significant difference was found between sites, apart from the southern anticyclonic eddy (A2), where the GCP rate (180.2 ± 32.0 mmol O_2 m^{-2} d^{-1}) was significantly greater than GCP rate at the cyclonic eddy (C4) (116.5 ± 18.2 mmol O_2 m^{-2} d^{-1}), (t = 4.9, p < 0.05, df = 7), characterized by the lowest DIN concentration and the lowest Z_m (Table 1).

[24] In late summer, GCP and DCR rates were much lower than in spring; nevertheless mesoscale variability was observed between sites. Both rates decreased from the anticyclonic eddy (63 mmol O_2 m^{-2} d^{-1} and −58 mmol
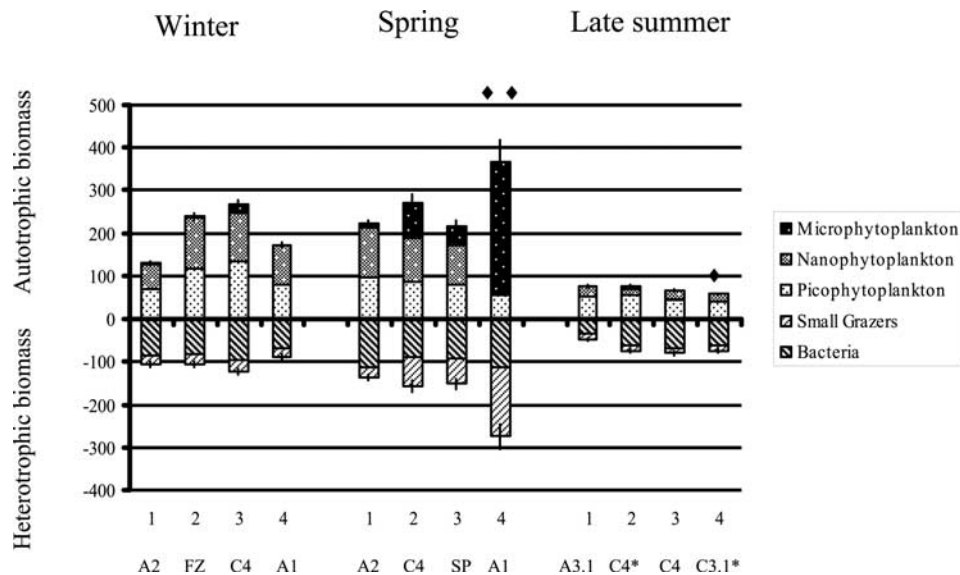
Figure 4. Integrated biomass of the autotrophic and heterotrophic microbial organisms during winter, spring, and late summer. The hydrodynamical structure identification is mentioned above the site number (C4 and C3-1, cyclonic eddies; A1, A2, and A3-1, anticyclonic eddies; FZ, frontal zone; SP, saddle point; an asterisk indicates that measurements were made in the vicinity of the associated hydrodynamical structure). Diamonds indicate no measure of microphytoplankton; double diamonds indicate no measure of pico- and nanophytoplankton.

$O_2 \, m^{-2} \, d^{-1}$) to the cyclonic eddy (C4) (26 mmol $O_2 \, m^{-2} \, d^{-1}$ and -45 mmol $O_2 \, m^{-2} \, d^{-1}$ for GCP and DCR, respectively). However, in the vicinity of C3-1, some surprisingly large rates of GCP (294 mmol $O_2 \, m^{-2} \, d^{-1}$) and DCR (-266 mmol $O_2 \, m^{-2} \, d^{-1}$) were observed, due to large values of oxygen decrease in dark samples. These rates were thus omitted from the present study because it could not be determined if these high values were due to contamination, analytical problems in that data set or to an unusual biological activity. It is worth noting that this area does not present any unusually high nutrient concentration, temperature, chlorophyll *a* concentration, primary production rates [*Karayanni et al.*, 2005; *Leblanc et al.*, 2005], bacterial production rates (data not published) or differences in the microbial community structure.

3.3. Autotrophic and Heterotrophic Biomasses

[25] In winter, the integrated microbial community biomass was dominated by autotrophic organisms in the southern anticyclonic eddy (A2), frontal zone and cyclonic eddy (C4) (Figure 4). It should be noted that for the northern anticyclonic eddy (A1), the microphytoplanktonic biomass was not determined (lost samples), and only Synechococcus data were available. The microbial community, in carbon units, was made up of 55% of autotrophs and 45% of heterotrophs. The picophytoplankton and nanophytoplankton community represented 45–55% each of the autotrophic community, whereas the microphytoplankton was never greater than 7% of this community. The bacteria community represented around 80% of the heterotrophic biomass at all sites, and the micrograzers contributed to 20%. The frontal zone was associated with high GCP and DCR values (Figure 3), and recorded the maximum concentrations in autotrophic and heterotrophic biomasses (respectively

238.3 mmol C m^{-2} and 105.4 mmol C m^{-2}). Interestingly, the cyclonic structure (C4) presented high GCP and autotrophic biomass concentration (266.8 mmol C m^{-2}) whereas A1 recorded the lowest DCR value and heterotrophic biomass concentration (88.5 mmol C m^{-2}).

[26] In spring, the integrated microbial community biomass (Figure 4) was dominated by autotrophic biomass (ranging from 57 to 63% of the contribution to the total community). Microphytoplankton was highly variable between sites, driven by a latitudinal gradient, contributing to <4% of the autotrophic biomass at the anticyclonic eddy (A2), 30% and 21% at the vicinity of C4 and SP. Despite missing data at A1, the microphytoplankton biomass was so high that even with only these data the autotrophic biomass calculated (497 mmol C m^{-2}) was much higher than at the three other sites. The large contribution of diatoms at this site also coincided with the highest heterotrophic biomass measured (dominated by ciliates and tintinnids). The anticyclonic eddy (A1) situated in the north of the study area, where the highest DIN concentrations and the deepest Z_m (Table 1) were also recorded. The biomass of microphytoplankton was mainly responsible for the variability of autotrophic biomass between the spring sites. Thus it was at (A2) in the southern area, were the pool of microphytoplankton was low, that the lowest autotrophic biomasses were found (214 mmol C m^{-2}). At this site, the lowest DIN concentration and the shallower Z_m were recorded (Table 1).

[27] In late summer, the autotrophic ranged from 57.8 to 76.0 mmol C m^{-2} and the heterotrophic biomass ranged from 46.1 to 79.8 mmol C m^{-2}. The variability of heterotrophic biomasses was mainly due to that of bacterial biomass, whose contribution ranged from 70 to 87% of the heterotrophic community biomass. It was greater
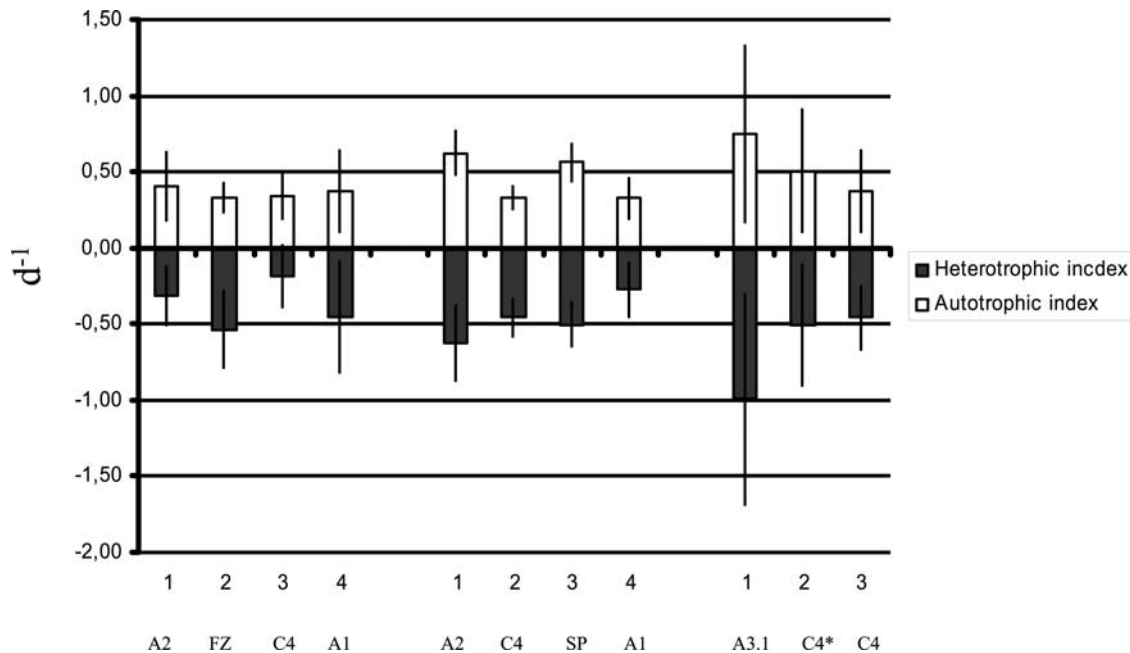
Figure 5. Flux to biomass ratios (d^{-1}): GCP/autotrophic biomass and DCR/heterotrophic biomass for winter spring and late summer at four different sites. Diamonds indicate no measure of microphytoplankton; double diamonds indicate no measure of pico- and nanophytoplankton. An asterisk indicates that measurements were made in the vicinity of the associated hydrodynamical structure.

(79.8 mmol C m^{-2}) in the cyclonic eddy C4 in which we recorded the highest value of DIN (Table 1).

3.4. Autotrophic and Heterotrophic Indices

[28] In winter, the autotrophic index was constant over the three sites (A2, frontal zone, C4) where this value could be determined and averaged 0.36 ± 0.04 d^{-1} (Figure 5). Thus at these three sites biomass and GCP fluxes varied in the same way. Although the mean index decreased from winter to spring (0.51 ± 0.16 d^{-1}, 0.46 ± 0.16 d^{-1}, respectively, including site A1) the difference was not significant ($t = 0.24$; $p = 0.83$; $n = 2$), due to a great variability of the index in spring. The highest value (0.64 d^{-1}) was recorded in the southern anticyclonic eddy A2 in the southern area where the lowest DIN concentration and shallower Z_m were found (Table 1). Although at the anticyclonic eddy (A1), only microphytoplankton data were available for the autotrophs, the autotrophic index was considered since almost all the primary production was due to diatoms [*Leblanc et al.*, 2005]. This value was particularly low (0.3 ± 0.1 d^{-1}). Finally, in fall, the autotrophic index increased further with a value of 0.54 ± 0.19 d^{-1} (Figure 5).

[29] In winter, the heterotrophic index averaged 0.37 ± 0.16 d^{-1}. The lowest value (0.18 d^{-1}) was recorded in the cyclonic eddy C4 (site 3, Figure 5), and the highest value (0.54 d^{-1}) was recorded in the frontal zone. In spring, the heterotrophic index averaged 0.47 ± 0.15 d^{-1}. The lowest value (0.38 d^{-1}) was recorded in the anticyclonic eddy (A1) in the northern area and associated with the highest value of DIN and Z_m (Table 1). In late summer, the heterotrophic index was averaged 0.65 ± 0.30 d^{-1}. The lowest value (0.46 d^{-1}), coincident with the lowest autotrophic index,

was observed in the cyclonic eddy C4, where the surface DIN concentrations were still not depleted, in contrast with the other sites (Table 1).

3.5. Statistical Analysis

[30] The PCA is used to describe within a two-dimensional space the linear covariability of the observed variables. In this study, we present only the representation of the two main factors, which account for over 50% of total variance. We have arbitrarily chosen not to take into account any variable which coordinates were less than 0.5 to an axis, and it is not thought to have a significant part in explaining the variance summarized by the axis (shaded box in Figure 6).

[31] In winter, the first two factors in PCA accounted for 59.1% of the variance (factor 1, 35.3%; factor 2, 23.8 %; $df = 54$; $p < 0.001$). The main axis accounts for the covariability between the GCP rates, the micrograzers and the depth. The second axis accounts for the covariability between inorganic nutrients and temperature, and to a lesser extent the second axis accounts for the covariability between the microphytoplankton and picophytoplankton as well as depth (Figure 6a).

[32] In spring, the first two factors accounted for 85.6% of the variance (factor 1, 66.4%; factor 2, 19.2%; $df = 54$; $p < 0.001$). The main axis accounts for the covariability of the GCP, DCR rates, the nanophytoplankton, picophytoplankton, bacteria, nutrients, depth, temperature, also to a lesser extent the main axis accounts for the covariability of the microphytoplankton and micrograzers. The second axis describes the covariability of the microphytoplankton and micrograzers and temperature (Figure 6b).

[33] In late summer, the first two factors accounted for 66.1% of the variance (factor 1, 41.4%; factor 2, 24.7%; $df =$
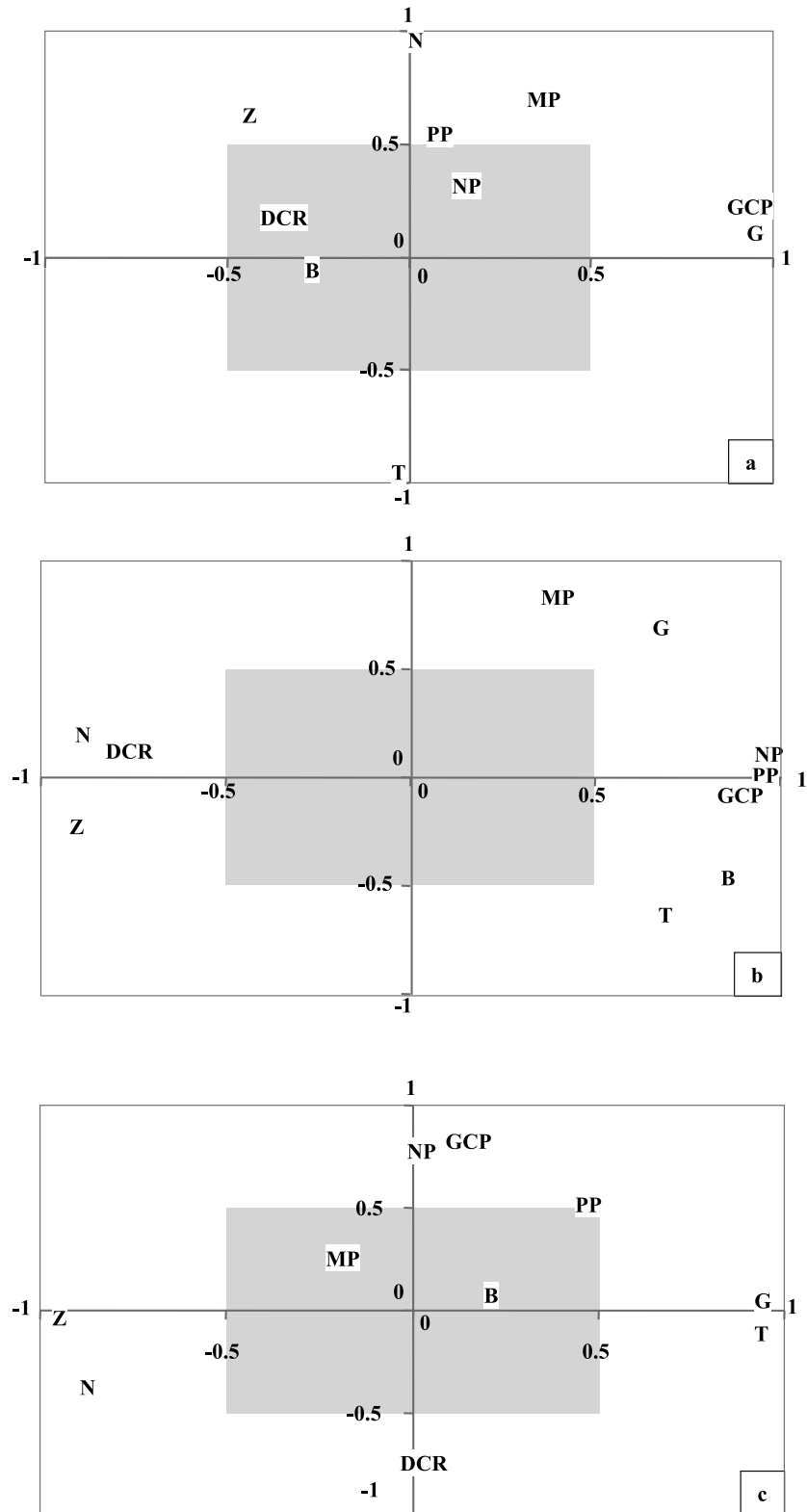
Figure 6. Principal component analysis results for POMME 1, 2, and 3 cruises. Abbreviations are as follows: MP, microphytoplanton; NP, nanophytoplankton; PP, picophytoplankton; G, micrograzers; B, bacteria; GCP, gross community production; DCR, dark community respiration; T, temperature; Z, depth; N, dissolved inorganic nitrogen. Axes are factor 1 and 2 of the PCA, respectively. The shaded area expresses a nonsignificant contribution to the explained variance, arbitrary criteria.
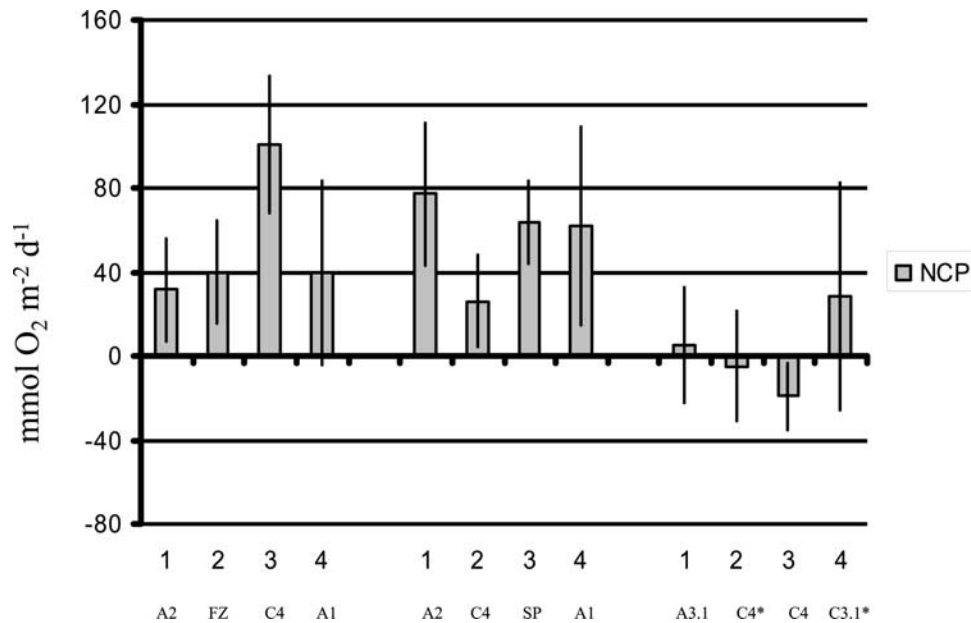
Figure 7. Integrated net community production fluxes (mmol O_2 m^{-2} d^{-1}) in the upper 100 m at four sites situated in different hydrodynamical structures (Table 1) during winter, spring, and late summer. The hydrodynamical structure identification is mentioned above the site number.

54; $p < 0.001$). The main axis accounts for the covariability of the micrograzers, temperature and inorganic nitrogen. The second axis is describing the covariability of GCP and DCR rates, and the nanophytoplankton (Figure 6c).

4. Discussion

4.1. Trophic Status of the Study Area

[34] The study area is both within the NADR and at the transition zone between NADR and the North Atlantic Subtropical Gyre (NASE) provinces [*Longhurst et al.*, 1995]. In 2001, the POMME area clearly showed a seasonal cycle (Figure 7) with an ecosystem dominated by autotrophy in winter (NCP: 52.9 ± 31.9 mmol O_2 m^{-2} d^{-1}) and spring (NCP: 57.2 ± 21.9 mmol O_2 m^{-2} d^{-1}) and a balanced system during late summer (NCP: 2.4 ± 20.0 mmol O_2 m^{-2} d^{-1}). These results contrast with values obtained from previous studies conducted in the NASE province situated south of the study area. The NASE province in the eastern Atlantic Ocean was dominated by net heterotrophy during summer 1998 (NCP: −129 ± 18 mmol O_2 m^{-2} d^{-1}), by a balanced system during spring 1999 (NCP: −13 ± 19 mmol O_2 m^{-2} d^{-1} [*González et al.*, 2001]) and net heterotrophy in September 2000 (NCP: −33 ± 14 mmol O_2 m^{-2} d^{-1} [*Serret et al.*, 2002]). The annual budget within POMME area, was estimated using linear interpolation between sampling dates. Thus the mean annual NCP rate in the upper 100 m would correspond to 33 ± 19 mmol O_2 m^{-2} d^{-1}, which is a potential carbon sink for the atmosphere.

4.2. Sources of Variability

[35] Sources of variability of fluxes can be explored more carefully in our study where sampling partially achieved mesoscale level during the legs 1. This earlier sampling provided with the environmental description for the selected sites of legs 2, where process studies were carried out for 48 hours.

[36] During the leg 1 of the winter cruise, chlorophyll concentrations and nitraclines were observed almost at all sites at greater depth than 100 m depth [*Claustre et al.*, 2005; *Fernández et al.*, 2005a], suggesting deep mixed layers and strong light limitation just before the leg 2 of the winter cruise. At the start of leg 2 (1–17 March) the ecosystem was still rich in nutrients (Table 1). The community structure was mainly composed of pico- and nano-phytoplankton (Figure 4), and GCP was covarying mostly with the micrograzers (Figure 6), suggesting a top down control on small autotrophic biomass. Profiles of micro-grazer biomass were homogeneous over the upper 100 m [*Karayanni et al.*, 2005], indicating that the ecosystem was at an early stage in ecological succession [*Legendre and Rassoulzadegan*, 1995; *Duarte et al.*, 2000]. However the system was already clearly autotrophic during leg 2 of the winter cruise (mean NCP: 52.9 ± 31.9 mmol O_2 m^{-2} d^{-1}). These data are consistent with noticeable increases of integrated chlorophyll with time within the euphotic zone during leg 2 [*Claustre et al.*, 2005], and primary production based on ^{14}C data [*Karayanni et al.*, 2005], which confirm a bloom initiation. However, there was a great variability around the mean value of NCP. We previously reported that the horizontal distributions of GCP and DCR at 5 m were constrained by hydrodynamical structures [*Maixandeau et al.*, 2005]. This is confirmed by the depth integrated values of GCP rates, DCR rates and microbial biomass presented in Figures 3 and 4. GCP and autotrophic biomass were higher in the cyclonic eddy (C4) and in the frontal zone. This is consistent with earlier observations [*Falkowski et al.*, 1991; *Oschlies and Garçon*, 1998; *Rodríguez et al.*, 2001; *Sournia et al.*, 1990]. On the other hand, autotrophic indices do not vary between sites suggesting that the growth rate of the autotrophic community is not controlled by the hydro-

dynamical context. The consistency of this ratio within the range of variation of the autotrophic biomass (100% variation between site 1 and site 3), and the range of variation of GCP rates (60%) seems to indicate a close coupling between the autotrophic biomass and its related rate, independently of the hydrological context. Heterotrophic biomass, DCR fluxes and heterotrophic index are lower in the cyclonic eddy C4. At this site bacterial respiration is almost completely responsible for DCR [*Maixandeau et al.*, 2005; F. van Wambeke et al., manuscript in preparation, 2005], this suggest that bacterial remineralization processes are reduced. This could be explained by the time required for bacteria to reduce organic matter [*Blight et al.*, 1995], as the freshly produced organic matter is advected out of the cyclonic eddy by divergent currents [*Maixandeau et al.*, 2005]. Thus in winter a disequilibrium between GCP and DCR is enhanced in the cyclonic eddy (C4) due to the delayed process of mineralization by bacteria, and consequently a high value of NCP was recorded (Figure 7).

[37] The time period in which leg 2 of the spring cruise occurred (18 April–2 May) corresponded roughly to a plateau phase in chlorophyll accumulation within Z_e [*Claustre et al.*, 2005]. Maximum primary production was reached at the end of the leg 1, in the southwestern part of anticyclonic eddy A2 (up to 300 mmoles C m^{-2} d^{-1}, data based on ^{13}C measurements [*Fernández et al.*, 2005b]). During leg 2, observations indicate a clear contrast in microbial biomass and structure between two sites situated within an anticyclonic eddy, but in the northern (site 4, A1) and southern (site 1, A2) areas respectively (Figure 4). Indeed, at A1, high values of microphytoplankton biomass were observed, mainly diatoms [*Leblanc et al.*, 2005] associated with high heterotrophic ciliates biomass [*Karayanni et al.*, 2005]. In contrast to this variability, rates of GCP and DCR are surprisingly constant over the area (Figure 3), and could be due to a light reduction under cloudy conditions. Actually, the bloom started earlier in the southern area due to earlier stratification of the winter mixed layer, and thus production was greater in the south until depletion of nutrients [*Maixandeau et al.*, 2005; *Lévy et al.*, 2005]. During leg 2 investigations of the different sites were made from the southern to the northern part. This sampling strategy implied that the latitudinal evolution of the ecosystem and the observations were concomitant and therefore reduced the apparent time lag observed in stratification between the north and the south. Despite this temporal transition, the ecosystem sampled in the south is nutrient limited resulting from a shallow Z_m, and the ecosystem in the north is constrained by the light availability due to a Z_m deeper than the Z_e. Light (e.g., depth) and nutrients are anticorrelated with the GCP and autotrophic biomass (Figure 6), exhibiting the depletion of nutrients and light limitation. The stratification is now covarying with rates, indicating that the stratification of the water column and that the activity is mainly constrained within the mixed layer. This is consistent with the study of *Lévy et al.* [2005], which is based on satellite data and model outputs. However, the study of *Paci et al.* [2005] based on a model output, shows not only that the Z_m is deeper in the north than in the south, but is also filament-shaped which seems to "result from the interplay between the atmospheric forcing and the deformation induced by mesoscale eddies" [*Paci et al.*, 2005,

section 4.4, paragraph 3]. In this study, the microphytoplankton biomass presents clear mesoscale variability between sites, which is probably the result of the different bloom stages induced by the mesoscale features [*Karrasch et al.*, 1996].

[38] At the anticyclonic gyre A1 (site 4) DCR and GCP fluxes were not enhanced in the same proportions than autotrophic and heterotrophic biomasses and consequently the autotrophic and hetrotrophic indices were low. This would suggest that the microphytoplankton growth rate was lower than that of smaller autotrophs. However, this is not the general conclusion obtained from the analysis of photosynthesis-irradiance curves and diagnostic pigments, combined for bio-optical modelling of primary production [*Claustre et al.*, 2005]. These authors showed that, under equal conditions of irradiance and chlorophyll biomass, carbon fixation would be twice higher when diatoms dominate the community. This is in accordance with the recognized opportunistic status of bigger phytoplantonic cells like diatoms, which generally proliferate under good conditions of light and nutrients. The cloudiness was highly variable during the cruise, and indeed the observed PAR at A1 (site 4) was only 53% of what it would have been on a sunny day. Similar cloudy conditions were met at the cyclonic eddy C4 where the daily irradiance was only 52% of the one occurring on a sunny day. This confirms that GCP could have been much higher at these sites. Finally, the low heterotrophic index obtained at the site 4 (anticyclonic eddy A1) confirms that DCR was not greatly affected by the blooms of tintinnids that were taking place, representing twice the bacteria stocks, because microzooplankton respire, per unit biomass, much less than heterotrophic bacteria. In spring, stratification appeared to be temporally variable and modulated by mesoscale structures (Table 1) and stratification was also the main controlling factor in ecosystem functioning. However, the mesoscale effects were finally more easily observed on biomass structures, which integrate past events, than from a single profile of GCP and DCR which was measured in highly variable conditions of cloudiness.

[39] In late summer, the microbial community was adapted to nutrient limitation (Table 1) and dominated by small cells (Figure 4) whose surface-to-volume ratio is high and enhances the uptake of dissolved nutrients [*Chisholm*, 1992]. Micrograzers were only present in mixed layer, and we observed an uncoupling the variabilities of environmental variables, rates and micro-organisms biomasses (Figure 6). Covariability between nanophyhtoplanktonic biomass and GCP rates contrasted with the lack of covariability between GCP and other phytoplanktonic biomasses, probably because (1) there was a limited range of phytoplanktonic biomasses and (2) in a system functioning on nutrient regeneration, direct correlations between stocks should be reduced, due to the different timescales involved in each processes. It is interesting to note, however, that the covariability between GCP and DCR greatly increased from spring to fall (Figure 6), which is also in agreement with strong interactions between mineralization, i.e., regeneration fluxes, and primary production. Mesoscale variability was not clearly evidenced from Figures 3 and 4 as the microbial community biomass and fluxes were low. However, DIN in the mixed layer was greater within the

cyclonic eddy (C4, Table 1) which could be due to nutrient injection [*Falkowski et al.*, 1991; *McGillicuddy et al.*, 1998; *Oschlies and Garçon*, 1998; *Fernández et al.*, 2005a]. This indicates that the ecosystem was not exclusively sustained by regenerated nutrients at this site. Interestingly, the cyclonic eddy (C4) was characterized by lower autotrophic and heterotrophic indices (Figure 5), i.e., slow growth and decay rates. In this case, daily irradiance, equal at the site A3-1 and C4, was not a sufficient explanation to justify the autotrophic index decrease. Since mesoscale features constrain the stratification [*Karrasch et al.*, 1996], the cyclonic eddy could have delayed the ecosystem development, by dispersing the biogeochemical resources produced at its edges through filament formation [*Lima et al.*, 2002].

4.3. Conclusions

[40] For all seasons, the variability in GCP and DCR did not follow the same pattern as microbial biomass and structure. The information given by the microbial community structure is integrated a large period of time and could mirror past events, whereas biological fluxes are representative of the instantaneous ecosystem functioning. Mesoscale structures controlled spatial variability of the biological processes in winter, which were characterized by an increase in net autotrophy at the cyclonic eddy. In spring, the ecosystem was in a transient state due to delayed stratification in the north, which is modulated by the mesoscale structures. However the variability in cloudiness probably led to constant biological fluxes throughout the sites; in late summer, in spite of weak variability and strong stratification, the cyclonic eddy (C4) delayed the evolution of the ecosystem. Finally, this study highlights that small organisms (picoautotrophs, nanoautotrophs, and bacteria) are the main organisms contributing to biological fluxes throughout the year and that episodic blooms of microphytoplankton are related to mesoscale structures.

References

Arhan, M., A. Colin de Verdière, and L. Mémery (1994), The eastern boundary of the subtropical North Atlantic, *J. Phys. Oceanogr.*, *24*, 1295–1316.

Armstrong, F. A. J., C. R. Stearns, and J. D. H. Strickland (1967), The measurement of upwelling and subsequent biological processes by means of the Technicon AutoAnalyzer and associated equipment, *Deep Sea Res.*, *14*, 381–389.

Assenbaum, M., and G. Reverdin (2005), Near real-time analyses of the mesoscale circulation during the POMME experiment, *Deep Sea Res., Part I*, in press.

Azam, F., T. Fenchel, J. G. Field, J. S. Gray, L. A. Meyer-Reil, and F. Thingstad (1983), The ecological role of water-column microbes in the sea, *Mar. Ecol. Prog. Ser.*, *10*, 257–263.

Blight, S. P., T. L. Bentley, D. Lefèvre, C. Robinson, R. Rodrigues, J. Rowlands, and P. J. L. B. Williams (1995), Phasing of autotrophic and heterotrophic plankton metabolism in a temperate coastal ecosystem, *Mar. Ecol. Prog. Ser.*, *128*, 61–75.

Børsheim, K. Y., and G. Bratbak (1987), Cell volume to cell carbon conversion factors for bacterivorous *Monas* sp. enriched from sea water, *Mar. Ecol. Prog. Ser.*, *36*, 171–175.

Caillau, C., H. Claustre, F. Vidussi, D. Marie, and D. Vaulot (1996), Carbon biomass, and growth rates as estimated from ^{14}C pigment labelling, during photoacclimatation in Prochlorococcus CCMP 1378, *Mar. Ecol. Prog. Ser.*, *145*, 209–221.

Caron, D. A., H. G. Dam, P. Kremer, E. J. Lessard, L. P. Madin, T. C. Malone, J. M. Napp, E. R. Peele, M. R. Roman, and M. J. Youngbluth (1995), The contribution of microorganisms to particulate carbon and nitrogen in surface waters of the Sargasso Sea near Bermuda, *Deep Sea Res., Part I*, *42*, 943–972.

Chisholm, S. W. (1992), Phytoplankton size, in *Primary Production and Biogeochemical Cycles in the Sea*, pp. 213–238, A. Woodhead, New York.

Claustre, H., M. Babin, D. Merien, J. Ras, L. Prieur, S. Dallot, O. Prasil, H. Dousova, and T. Moutin (2005), Toward a taxon-specific parameterization of bio-optical models of primary production: A case study in the North Atlantic, *J. Geophys. Res.*, *110*, C07S12, doi:10.1029/2004JC002634.

Cotner, J. B., and B. A. Biddanda (2002), Small players, large role: Microbial influence on biogeochemical processes in Pelagic aquatic ecosystems, *Ecosystems*, *5*, 105–121.

Cullen, J. J., P. J. S. Franks, D. M. Karl, and A. Longhurst (2002), Physical influences on marine ecosystem dynamics, in *The Sea*, edited by B. J. Rothschild, pp. 297–336, John Wiley, Hoboken, N. J.

del Giorgio, P. A., and C. M. Duarte (2002), Respiration in the open ocean, *Nature*, *420*, 379–384.

del Giorgio, P. A., J. C. Jonathan, and A. Cimbleris (1997), Respiration rates in bacteria exceed phytoplankton production in unproductive aquatic systems, *Nature*, *385*, 148–151.

Duarte, C. M., and S. Agusti (1998), The CO2 balance of unproductive aquatic ecosystems, *Science*, *281*, 234–236.

Duarte, C. M., S. Agustí, and N. S. R. Agawin (2000), Response of a Mediterranean phytoplankton community to increased nutrient inputs: A mesocosm experiment, *Mar. Ecol. Prog. Ser.*, *195*, 61–70.

Dubreuil, C. (2003), Variabilité spatio-temporelle de l'ultraplancton dans le secteur indien de l'océan Austral: Sciences de l'environnement, Ph.D. thesis, Aix-Marseille II, Univ. de la Méditerranée, Marseille, France.

Falkowski, P. G., D. Ziemann, K. Kolber, and P. K. Bienfang (1991), Role of eddy pumping in enhancing primary production in the ocean, *Nature*, *352*, 55–58.

Fernández, I. C., P. Raimbault, G. Caniaux, N. Garcia, and P. Rimmelin (2005a), Influence of mesoscale eddies on nitrate distribution during the POMME program in the north-east Atlantic Ocean, *J. Mar. Syst.*, *55*, 155–175.

Fernández, C. I., P. Raimbault, N. Garcia, P. Rimmelin, and G. Caniaux (2005b), An estimation of annual new production and carbon fluxes in the northeast Atlantic Ocean during 2001, *J. Geophys. Res.*, *110*, C07S13, doi:10.1029/2004JC002616.

Field, C. B., M. J. Behrenfeld, J. T. Randerson, and P. Falkowski (1998), Primary production of the biosphere: Integrating terrestrial and oceanic components, *Science*, *281*, 237–240.

Gaarder, T., and H. H. Gran (1927), Investigations of the production of plankton in the Oslo Fjord, *Rapp. Proc. Verb. Cons. Int. Explor. Mar.*, *42*, 1–48.

Gaillard, F., H. Mercier, and C. Kermabon (2005), A synthesis of the POMME physical data set: One year monitoring of the upper layer, *J. Geophys. Res.*, *110*, C07S07, doi:10.1029/2004JC002764.

Gasol, J. M., and C. M. Duarte (2000), Comparative analyses in aquatic microbial ecology: How far do they go?, *FEMS Microbiol. Ecol.*, *31*, 99–106.

Geider, R. J. (1997), Photosynthesis or planktonic respiration?, *Nature*, *132*, 1038.

González, N., R. Anadón, B. Mouriño, B. Sinha, J. Escanez, and D. de Armas (2001), The metabolic balance of the planktonic community in the North Atlantic Subtropical Gyre: The role of mesoscale instabilities, *Limnol. Oceanogr.*, *46*, 946–952.

González, N., R. Anadón, and E. Maranon (2002), Large-scale variability of planktonic net community metabolism in the Atlantic Ocean: Importance of temporal changes in oligotrophic subtropical waters, *Mar. Ecol. Prog. Ser.*, *233*, 21–30.

Grégori, G. (2001), Ultraplancton dans la baie de Marseille: Séries temporelles, viabilité bactérienne et mesure de la respiration par cytométrie en flux: Sciences de l'environnement marin, Ph.D. thesis, Aix Marseille II, Univ. de la Mediterranée, Marseille, France.

Kana, T. M., and P. M. Glibert (1987), Effect of irradiance up to 2000 μEm-2 s-1 on marine Synechococcus pigmentation, and cell composition, *Deep Sea Res., Part A*, *34*, 479–495.

Karayanni, H. (2004), Role des nanoflagellés hétérotrophes et des ciliés dans la régulation du pico- et nanoplancton photosynthétiques et des

bactéries en Atlantique NE et le recyclage de la matière organique, Ph.D. thesis, Sci. de l'Environ., Aix-Marseille, Univ. de la Méditerranée, Marseille, France.

Karayanni, H., U. Christaki, F. Van Wambeke, M. Denis, and T. Moutin (2005), Influence of ciliated protozoa and heterotrophic nanoflagellates on the fate of primary production in the northeast Atlantic Ocean, *J. Geophys. Res.*, 110, C07S15, doi:10.1029/2004JC002602.

Karrasch, B., H. G. Hoppe, S. Ullrich, and S. Podewski (1996), The role of mesoscale hydrography on microbial dynamics in the northeast Atlantic: Result of a spring bloom, *J. Mar. Res.*, 54, 99–122.

Laws, E. A. (1991), Photosynthetic quotients, new production and net community production in the open ocean, *Deep Sea Res., Part A*, 38, 143–167.

Leblanc, K., A. Leynaert, I. C. Fernandez, P. Rimmelin, T. Moutin, P. Raimbault, J. Ras, and B. Quéguiner (2005), A seasonal study of diatom dynamics in the North Atlantic during the POMME experiment (2001): Evidence for Si limitation of the spring bloom, *J. Geophys. Res.*, 110, C07S14, doi:10.1029/2004JC002621.

Legendre, P., and L. Legendre (1998), *Numerical Ecology*, 2nd Engl. ed., 853 pp., Elsevier, New York.

Legendre, L., and F. Rassoulzadegan (1995), Plankton and nutrient dynamics in marine waters, *Ophelia*, 41, 153–172.

Lévy, M., Y. Lehahn, J.-M. André, L. Mémery, H. Loisel, and E. Heifetz (2005), Production regimes in the northeast Atlantic: A study based on Sea-viewing Wide Field-of-view Sensor chlorophyll and ocean general circulation model mixed layer depth, *J. Geophys. Res.*, 110, C07S10, doi:10.1029/2004JC002771.

Lima, I. D., D. B. Olson, and S. C. Doney (2002), Biological response to frontal dynamics and mesoscale variability in oligotrophic environments: Biological production and community structure, *J. Geophys. Res.*, 107(C8), 3111, doi:10.1029/2000JC000393.

Longhurst, A., S. Sathyendranath, T. Platt, and C. Caverhill (1995), An estimate of global primary production in the ocean from satellite radiometer data, *J. Plankton Res.*, 17, 1245–1271.

Maixandeau, A., D. Lefèvre, C. I. Fernández, R. Sempéré, R. Fukuda-Sohrin, J. Ras, F. Van Wambeke, G. Caniaux, and B. Quéguiner (2005), Mesoscale and seasonal variability of community production and respiration in the NE Atlantic Ocean, *Deep Sea Res., Part I*, in press.

Margalef, R. (1978), Life forms of phytoplankton as survival alternatives in an unstable environment, *Oceanol. Acta*, 1, 493–509.

McGillicuddy, D. J., A. R. Robinson, D. A. Siegel, H. W. Jannasch, R. Johnson, T. D. Dickey, J. McNeil, A. F. Michaels, and A. H. Knap (1998), Influence of mesoscale eddies on new production in the Sargasso Sea, *Nature*, 394, 263–266.

Mémery, L., G. Reverdin, J. Paillet, and A. Oschlies (2005), Introduction to the POMME special section: Thermocline ventilation and biogeochemical tracer distribution in the northeast Atlantic Ocean and impact of mesoscale dynamics, *J. Geophys. Res.*, doi:10.1029/2005JC002976, in press.

Morel, A., and J. F. Berthon (1989), Surface pigments, algal biomass profiles and potential production of the euphotic layer: Relationships reinvestigated in view of remote sensing applications, *Limnol. Oceanogr.*, 34, 1545–1562.

Morel, A., and S. Maritorena (2001), Bio-optical properties of oceanic waters: A reappraisal, *J. Geophys. Res.*, 106, 7163–7180.

Oschlies, A., and V. Garçon (1998), Eddy-induced enhancement of primary production in a model of the North Atlantic Ocean, *Nature*, 394, 266–269.

Paci, A., G. Caniaux, M. Gavart, H. Giordani, M. Lévy, L. Prieur, and G. Reverdin (2005), A high-resolution simulation of the ocean during the POMME experiment: Simulation results and comparison with observations, *J. Geophys. Res.*, doi:10.1029/2004JC002712, in press.

Paillet, J., and M. Arhan (1996), Oceanic ventilation in the eastern North Atlantic, *J. Phys. Oceanogr.*, 26, 2036–2052.

Reverdin, G., M. Assenbaum, and L. Prieur (2005), Eastern North Atlantic Mode Waters during POMME (September 2000–2001), *J. Geophys. Res.*, 110, C07S04, doi:10.1029/2004JC002613.

Robinson, C., P. Serret, G. Tilstone, E. Teira, M. V. Zubkov, A. P. Rees, and E. M. S. Woodward (2002), Plankton respiration in the eastern Atlantic Ocean, *Deep Sea Res., Part I*, 49, 787–813.

Rodríguez, J., J. Tintoré, J. T. Allen, J. M. Blanco, D. Gomis, A. Reul, J. Ruiz, V. Rodríguez, F. Echevarría, and F. Jiménez-Gómez (2001), Mesoscale vertical motion and the size structure of phytoplankton in the ocean, *Nature*, 410, 360–363.

Serret, P., E. Fernández, J. A. Sostres, and R. Anadón (1999), Seasonal compensation of microbial production and respiration in a temperate sea, *Mar. Ecol. Prog. Ser.*, 187, 43–57.

Serret, P., E. Fernández, and C. Robinson (2002), Biogeographic differences in the net ecosystem metabolism of the open ocean, *Ecology*, 83, 3225–3234.

Sournia, A., J. M. Brylinski, S. Dallot, P. Le Corre, M. Leveau, L. Prieur, and C. Froget (1990), Fronts hydrologiques au large des côtes françaises: Les sites-ateliers du programme Frontal, *Oceanol. Acta*, 13, 413–438.

Strathmann, R. R. (1967), Estimating the organic carbon content of phytoplankton from cell volume or plasma volume, *Limnol. Oceanogr.*, 12, 411–418.

Throndsen, J. (1978), Preservation and storage, in *Phytoplankton Manual*, *Monogr. Oceanogr. Method.*, vol. 6, edited by A. Sournia, pp. 69–74, UNESCO, Paris.

Tréguer, P., and P. LeCorre (1975), Utilisation de l'AutoAnalyser II Technicon, in *Manuel d'analyse des sels nutritifs dans l'eau de mer*, 2nd ed., pp. 1–110, Univ. Bretagne Occident. Lab. de Chim. Mar., Brest, France.

Utermöhl, M. (1931), Über das umgekehrte mikroskop, *Arch. Hydrobiol. Planktol.*, 22, 643–645.

Williams, P. J. L. B. (1993), On the definition of plankton terms, *ICES Mar. Sci. Symp.*, 197, 9–19.

Williams, P. J. L. B. (1998), The balance of plankton respiration and photosynthesis in the open oceans, *Nature*, 394, 55–57.

Williams, P. J. L. B., and N. W. Jenkinson (1982), A transportable microprocessor-controlled precise Winkler titration suitable for field station and shipboard use, *Limnol. Oceanogr.*, 27, 576–584.

————————————

U. Christaki, Université du Littoral Côte d'Opale/Maison de la Recherche en Environnement Naturel, CNRS/INSU, UMR 8013 "Ecosystèmes Littoraux et Côtiers," 32 avenue Foch, F-62930 Wimereux, France. (urania.christaki@mren2.univ-littoral.fr)

M. Denis, H. Karayanni, D. Lefèvre, A. Maixandeau, M. Thyssen, and F. Van Wambeke, Laboratoire de Microbiologie, Géochimie et Ecologie Marines, Centre National de la Recherche Scientifique/Institut National des Sciences de l'Univers, UMR 6117, Centre d'Océanologie de Marseille, Université de la Méditerranée, Case 901, 163 avenue de Luminy, F-13288 Marseille Cedex 9, France. (denis@com.univ-mrs.fr; karayanni@com.univ-mrs.fr; lefevre@com.univ-mrs.fr; maixandeau@com.univ-mrs.fr; thyssen@com.univ-mrs.fr; wambeke@com.univ-mrs.fr)

C. I. Fernández, K. Leblanc, and B. Quéguiner, Laboratoire d'Océanographie et de Biogéochimie, Centre National de la Recherche Scientifique/Institut National des Sciences de l'Univers, UMR 6535, Centre d'Océanologie de Marseille, Université de la Méditerranée, 163 avenue de Luminy, F-13288 Marseille Cedex 9, France. (fernandez@com.univ-mrs.fr; leblanc@udel.edu; queguiner@com.univ-mrs.fr)

J. Uitz, Laboratoire d'Océanographie de Villefranche, Observatoire Océanologique, Quai de la Darse, B.P. 8, F-06238 Villefranche-sur-mer, France. (uitz@obs-vlfr.fr)